Experimental Investigation on the Application of Cold-mist Direct Evaporative Cooling in Data Centers

Ruiyong Mao[a,b], Hongwei Wu [c,*], Chao Li[a,**], Zujing Zhang[a], Xing Liang[d], Jiri Zhou[e], Jing Chen[f]

[a] College of Civil Engineering, Guizhou University, Guiyang, 550025, China
[b] Department of Building Science, School of Architecture, Tsinghua University, Beijing 100084, China
[c] School of Physics, Engineering and Computer Science, University of Hertfordshire, Hatfield AL10 9AB, United Kingdom
[d] School of Computer Science and Mathematics, Kingston University London, KT1 2EE, United Kingdom
[e] China MCC5 Group Co. LTD, MCC5 Tower, No. 9 Wuye Road, Jinjiang District, Chengdu, 610000, China
[f] Guizhou Industry Polytechnic College, Guiyang, 550025, China
E-mail addresses:
*Corresponding author: h.wu6@herts.ac.uk (H. Wu),
**Corresponding author: chaoli320@163.com (C. Li).
Tel: +44(0)1707284265 (H. Wu), +86 152 8503 5071 (C. Li).

Abstract: The rapid development of the internet era has driven the construction of numerous data centers worldwide. In hot climate, data centers consume significant energy for cooling. Cold-mist direct evaporative cooling offers a natural cooling solution that can help reduce this energy consumption. This study investigates the temperature and relative humidity changes of natural high-temperature air after being cooled using a cold-mist direct evaporative cooling test bench. The effects of several control factors such as spray angle, spray flow rate, and air speed on the cold-mist direct evaporative cooling performance was systematically examined. The findings revealed that: (1) the optimal spray angle for cold-mist direct evaporative cooling treatment air is 65°; (2) high-temperature air between 27 °C and 37 °C can be cooled to 23.57 °C to 25.58 °C after cold-mist direct evaporative cooling treatment, with relative humidity levels of 67.0% to 78.8%, meeting the air supply requirements for data centers; (3) the proposed approach could reduce the data center energy consumption by 14% to 41%, while extending the annual natural cooling period by 3.16% to 20.45%.

Keywords: Data center; Energy consumption; Free cooling; Evaporative cooling; Experiment

Nomenclature

c_{pa}	The specific heat capacity of air, kJ/(kg·°C)
c_{pm}	Air specific heat capacity at constant pressure, kJ/(kg·°C)
c_{pw}	The specific heat capacity water, kJ/(kg·°C)
dA	The heat and mass transfer area, m^2
G_a	The mass flow rate of air, kg/s
G_w	The mass flow rate of water, kg/s
h_d	The mass transfer coefficients between air and cold-mist, w/(m^2·°C), kg/(m^2·s)
h_s	The heat transfer coefficients between air and cold-mist, w/(m^2·°C), kg/(m^2·s)
m	Duct cross-sectional area, m^2
Q	Cooling capacity of CDEC, kW
Q_f	Energy consumption of the fan of the air supply system, kW
Q_p	Energy consumption of water pump, kW
Q_q	Latent heat exchange, kW
Q_x	Sensible heat exchange, kW
r	The latent heat of water evaporation, J/kg
t_a	The dry-bulb temperature of the air, °C
t_w	The temperature of the water, °C
Δt	Temperature difference between inlet and outlet air, °C
W	Energy consumption of air conditioning units, kW
Greek symbols	
φ_a	The air humidity, kg/kg (dry air)
φ_w	The air saturation humidity, kg/kg (dry air)
η	Refrigeration coefficient
v	Air speed, m/s
ξ	Energy saving rate
ρ	Air density, kg/m^3
Abbreviations	
CDEC	Cold-mist direct evaporative cooling
DC	DC
IAH	Inlet air relative humidity
IAT	Inlet air temperature
OAH	Outlet air relative humidity
OAT	Outlet air temperature

1. Introduction

Data centers (DCs) are significant energy consumers, accounting for approximately 1% to 1.5% of global electricity usage [1-3]. It is estimated that by 2022, DCs, along with cryptocurrencies and artificial intelligence (AI), will consume approximately 460 TWh of electricity globally, representing nearly 2% of total global electricity demand [4]. The primary energy consumers in DCs are information technology (IT) equipment and the associated heating, ventilation, and air conditioning (HVAC) systems [5,6]. In a typica DC, the largest share of energy consumption comes from the IT equipment load, which includes IT equipment (45%) and power distribution equipment (5%), while the cooling load follows closely, accounting for 38% of the total energy use [7-10]. The rapid expansion of data communications and computing has led to a substantial increase in energy consumption in DCs [11,12]. Cho et al. [13,14] forecasted that by 2030, DC power demand will rise to 2.13% of the world's electricity supply. It is therefore imperative to reduce the energy consumption in DCs.

Currently, most studies on reducing DC energy consumption focus on optimising the spatial layout and airflow management within DCs [15-18], as well as improving cold source management [19-22]. While these strategies enhance cooling efficiency and reduce energy consumption to some extent, they have limitations. It is widely recognized that utilizing natural cooling sources is an effective approach to further reducing energy consumption. Implementing natural cooling in DCs can significantly improve energy efficiency [23,24]. Jahangir et al. [25] found that free cooling systems could reduce DC cooling energy consumption by up to 47%. Similarly, Ding et al. [26] conducted an experimental study on a new DC cooling system that integrated heat recovery with free cooling. Their findings indicated that free cooling could be utilised for up to72.9% of the DC's operational time.

Direct air natural cooling technology leverages natural cooling sources to reduce energy consumption. When natural air is sufficiently cool, it can serve as a cooling medium for DCs [27]. However, the effectiveness of natural cooling is highly dependent on regional and climatic conditions [28]. In real-world applications, high temperature weather can limit the effectiveness of direct air cooling, making it insufficient to address DC cooling needs DCs. Evaporative cooling, on the other hand, is gaining recognition due to its ability to provide efficient cooling and ventilation [29-31]. J. Tissot et al. [32] conducted experiments on enhancing heat transfer in radiators using evaporative cooling through water jet airflow and found that injecting liquid droplets into the air reduced the airflow temperature under various conditions. Liu et al. [33] studied the combination of dew point evaporators with heat pipe technology in DCs, revealing that this combination can save nearly 90% of annual energy compared to traditional compression refrigeration. Additionally, spray precooling technology has been employed to cool the inlet air of natural draft dry cooling towers, effectively addressing performance degradation issues during high-temperature climate [34,35].

The application of evaporative cooling technology in DCs shows great potential for energy savings. Cao et al. [36] designed a falling film natural evaporative cooling system that efficiently dissipates heat generated inside the cabinet in real time, optimising energy use. Han et al. [37] proposed a novel water-cooled evaporative condenser, which was integrated into a composite air-conditioning system for DCs, achieving an average colling efficiency increase of 9.82%. Shao et al. [38] applied loop heat siphons with evaporative condensers to DCs, resulting in an extension of free cooling time by 7% to 14% annually. These studies demonstrate that evaporative cooling can significantly reduce energy consumption in DCs. However, previous research mainly focused on combining evaporative cooling with traditional cooling methods. This study explores the use of cold-mist direct evaporative cooling (CDEC) to cool high-temperature air, which is then delivered to DCs for equipment cooling.

By investigating innovative approaches to using CDEC in high-temperature climates, this research aims to enhance natural air cooling in DCs, providing an alternative cold source for improved energy efficiency.

The study also explores whether using CDEC to treat air in hot climates can provide natural cooling for DCs while reducing their energy consumption. To achieve this, a test bench was set up to analyze how high-temperature air changes after being cooled by CDEC and examined the effects of several key control parameters such as spray angle, air speed, and spray flow rate on high temperature air CDEC treatment. By exploring CDEC technology, we aim to address the cooling challenges faced by DCs in hot climates. Additionally, the study evaluates the cooling effectiveness, energy efficiency, and annual free cooling time of CDEC, providing insights into its cooling capacity and application advantages.

2. Experimental Details

2.1. Basic concepts of CDEC

CDEC involves the simultaneous heat and mass transfer between air and cold mist. Sensible heat transfer occurs when the air temperature is higher than the water temperature, while latent heat transfer takes place when there is a difference in moisture content between the air and the saturated air layer around the cold mist [39]. These heat and mass transfer processes interact and occur concurrently. Throughout the process, the air temperature decreases, humidity increases, and the cold mist temperature increases. To simplify the theoretical model of heat and mass transfer, the following assumptions are made:

(1) The constant Lewis number is equal to 1.0 [40].

(2) The heat and water required during the latent heat of evaporation process are provided by cold mist [41].

(3) The dry bulb temperature of saturated humid air has a linear relationship with humidity [42].

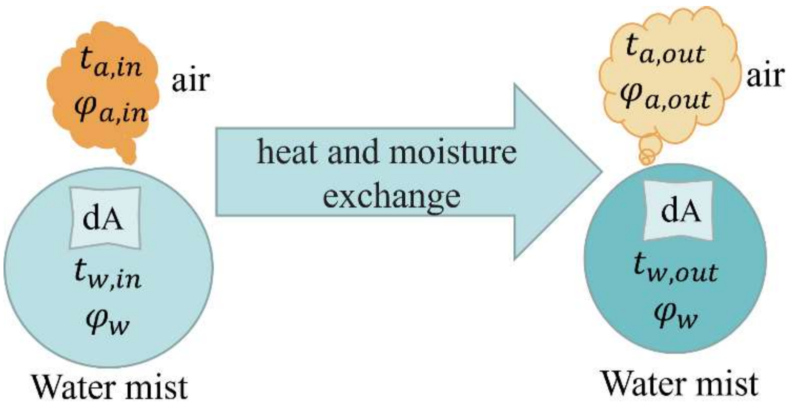

Fig. 1. The process of heat and mass transfer between air and cold-mist.

Fig. 1 illustrates the heat and humidity exchange process between air and cold mist. The heat transfer theory of CDEC can be described as follows: Eq. (1) represents the energy balance on the air side, where changes in air temperature are due to sensible heat transfer. Eq. (2) describes the variation in air humidity, which is influenced by the saturated wet air film surrounding the cold mist and the humidity difference between the air and the mist. Based on assumption (2), Eq. (3) represents the energy balance on the water side, accounting for the effects of temperature changes on both wet heat transfer and phase transition processes.

$$Q_x = G_a \cdot c_{pa} \cdot dt_a = h_s \cdot dA \cdot (t_a - t_w) \tag{1}$$

$$Q_q = G_a \cdot d\varphi_a = h_d \cdot dA \cdot (\varphi_w - \varphi_a) \tag{2}$$

$$G_w \cdot c_{pw} \cdot dt_w = h_s \cdot dA \cdot (t_a - t_w) - r \cdot h_d \cdot dA \cdot (\varphi_w - \varphi_a) \tag{3}$$

Where Q_x is the sensible heat exchange capacity, kW; Q_q is the latent heat exchange capacity, kW; G_a and G_w are the mass flow rates of air and water, kg/s; h_s and h_d are the heat transfer coefficients and mass transfer coefficients between air and cold-mist, w/(m^2·°C), kg/(m^2·s); r is the latent heat of water evaporation, J/kg; $\mathrm{t_a}$ and $\mathrm{t_w}$ are the dry-bulb temperature of the air and the temperature of the water, °C; φ_a and φ_w are the air humidity and saturation humidity, kg/kg (dry air); c_{pa} and c_{pw} are the specific heat capacity of air and water, kJ/(kg·°C); and dA is the heat and mass transfer area, m^2.

2.2. Experimental setup

Fig. 2 shows an image of the CDEC test bench. The test rig primarily consists of a spray chamber, a modular air-cooled heat pump unit, a control platform, an airspeed transmitter, temperature and humidity transmitter, a fan, and a rotameter. As depicted in Fig. 3, outdoor air enters the heating chamber through pipes and is heated by a heat exchanger. The temperature of the hot water supplied to the heat exchanger is adjusted via the KMS020DR-01 modular air-cooled heat pump unit to achieve the required air temperature for the experiment. The heated air is then sent to the spray chamber for CDEC cooling treatment. After cooling, the air is delivered to the computer room via the air supply system. Fig. 4 shows the control platform for the air conditioning unit and fan. The specific models, key parameters, measurement ranges, and accuracies of the main equipment are listed in Table 1.

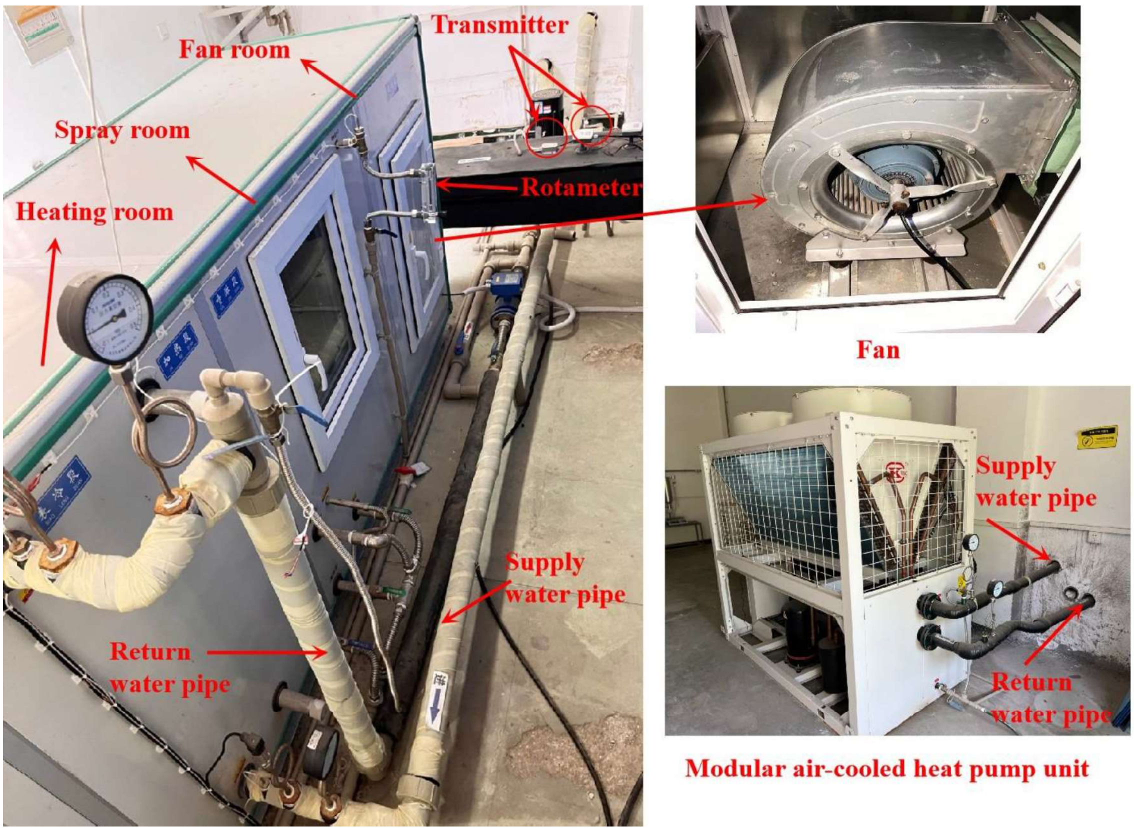

Fig. 2. Experimental setup diagram.

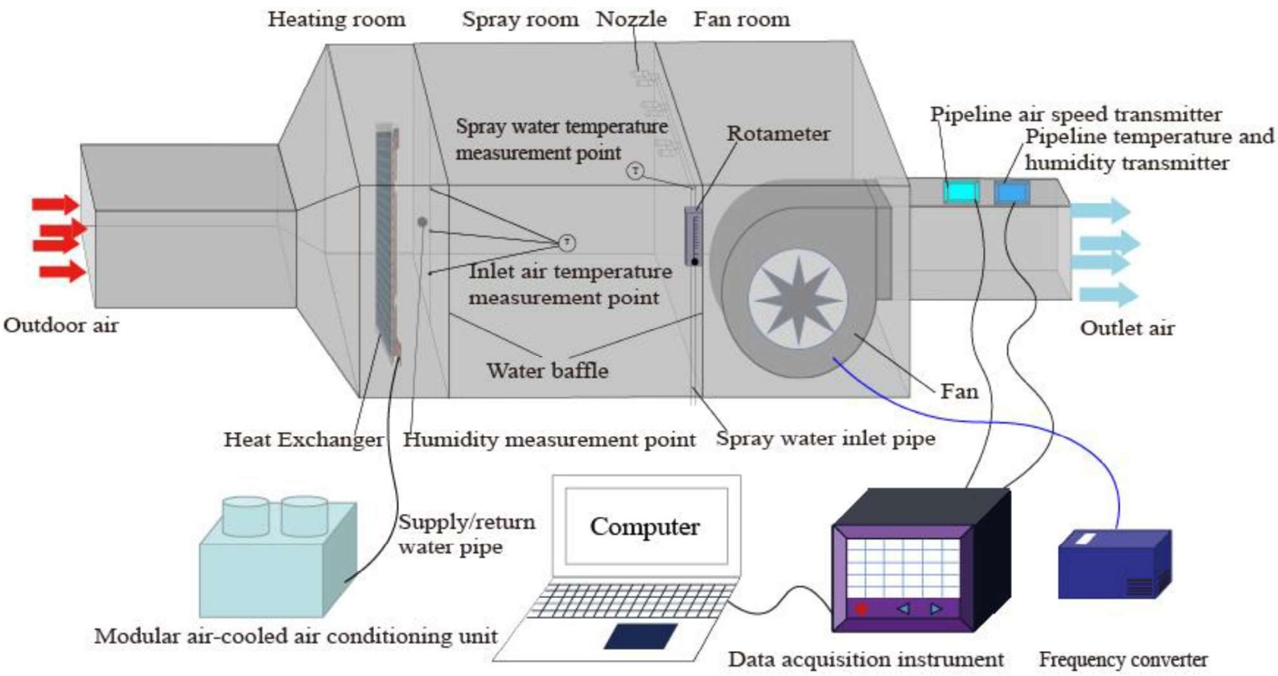

Fig. 3. Experimental schematic diagram.

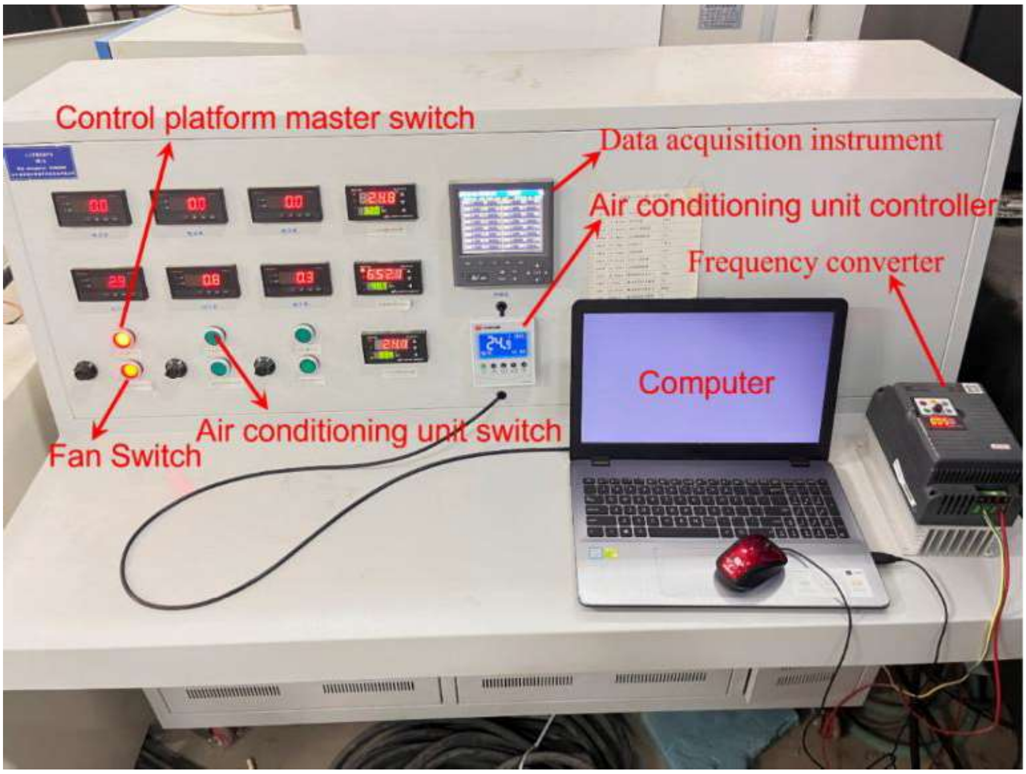

Fig. 4. Control platform.

Table 1. Main equipment technical parameter

Experiment equipment	Model	Parameters
Spray room	90cm×85cm×100cm	—
Fan room	60cm×85cm×100cm	—

Data acquisition instrument	SWP-ASR-MD	64 channels; Recording interval 20 seconds
Frequency converter	JT330S2	Input: three-phase AC380V 50 – 60 Hz Output: 4.0 kW G3/5.5 kW P3; 10A/13A 0 – 600 Hz
Pipeline air speed transmitter	PHF-F	Uncertainty: 0.02% Range: 0 – 30.00 m/s
Pipeline temperature and humidity transmitter	PWS-F	Uncertainty: ± 0.01 °C Range: -50 – 200 °C Uncertainty: ± 2% RH Range: 0 – 100% RH
Modular air-cooled heat pump unit	KMS020DR-01	Cooling capacity: 65 kW Refrigeration coefficient: 3.27 Heating capacity: 71 kW Heating coefficient: 3.60 Refrigerant: R22
Rotameter	DFA	Uncertainty: ± 4% Range: 0.2 – 1.8 L/min
Hygrometer	BY-2003HT	Uncertainty: ± 2% RH Range: 0 – 100% RH
Resistance thermometers	PT1000	Uncertainty: ± 0.01 °C Range: -50 – 200 °C
Nozzle	Aperture 1 mm	
Fan	YDW 3.0 - 4	1.5 kW; 1420 r/min

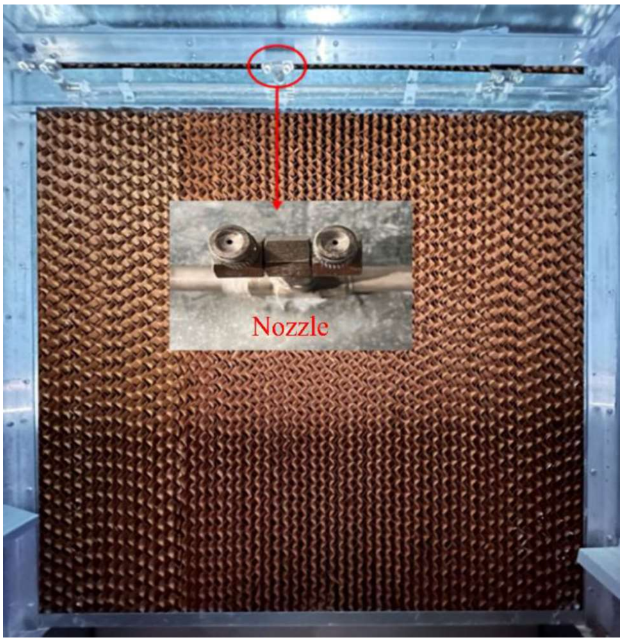

(a) Nozzle arrangement diagram

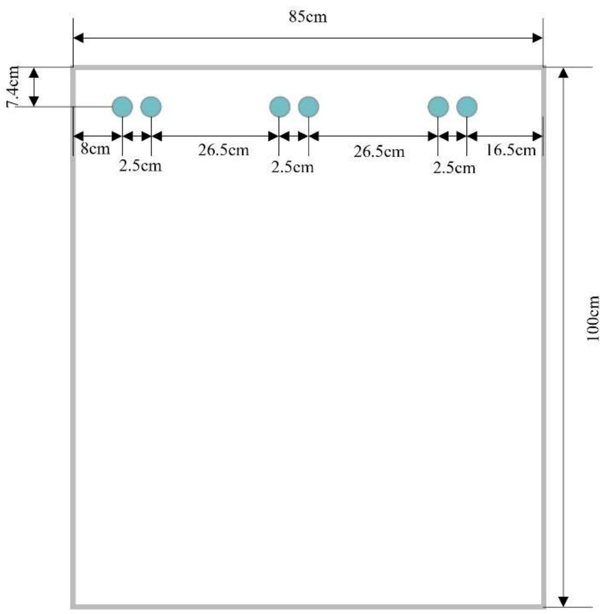

(b) Schematic diagram of nozzle arrangement

Fig. 5. Nozzle layout in the spray room.

Fig. 5 depicts the nozzle arrangement and its schematic within the spray chamber. In the current study, each nozzle has a diameter of 1 mm, with two nozzles spaced 2.5 cm apart to form a group, and each group spaced 26.5 cm apart. As shown in Fig. 5, the nozzles are positioned at the top of the air outlet side of the spray chamber, with the cold mist sprayed by the nozzles directed opposite to the airflow.

2.3. Measurement point layout

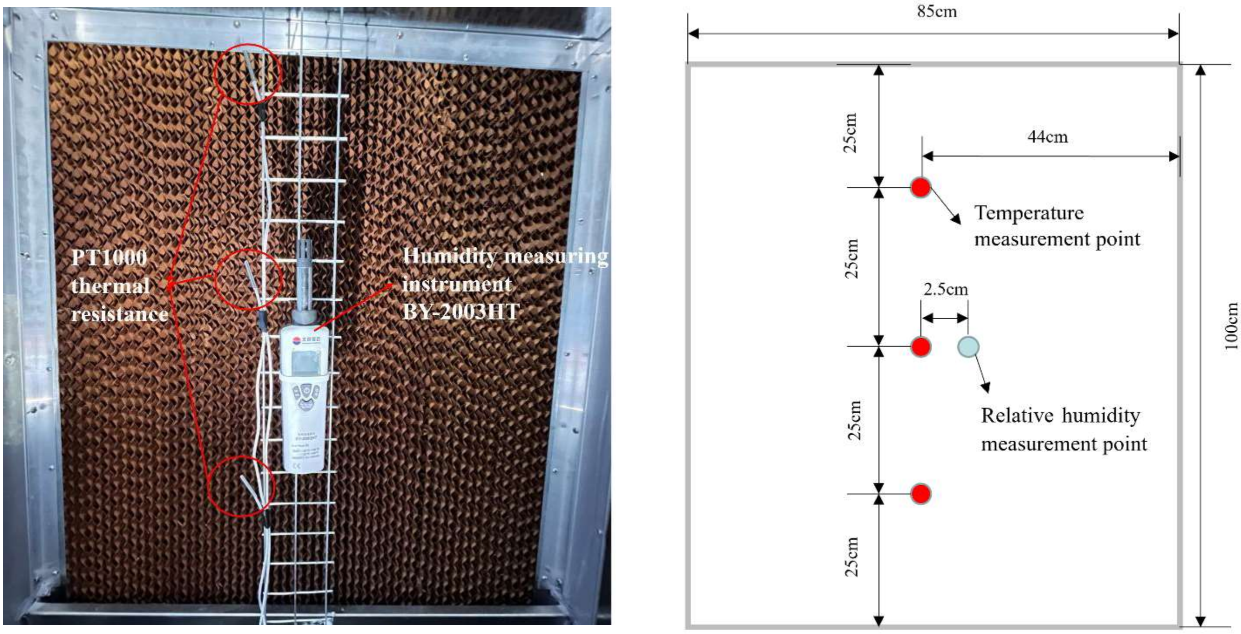

(a) Layout of temperature and humidity measurement points

(b) Schematic diagram of temperature and humidity measurement point layout

Fig. 6. Layout of IAT and IAH measurement points.

Fig. 6 shows the layout of the measurement points for inlet air temperature (IAT) and inlet air relative humidity (IAH) before CDEC treatment. These points are positioned on the partition between the heating chamber and the spray chamber. Fig. 6 (a) shows the spatial locations of temperature and relative humidity measurement points. To ensure accurate air temperature readings, three PT1000 thermistors are vertically and evenly spaced 25cm apart on the partition, as shown in Fig. 6(b). A relative humidity measurement point is located 2.5 cm away from the central temperature measurement point, with relative humidity measured using a Beijing BY-2003HT humidity sensor.

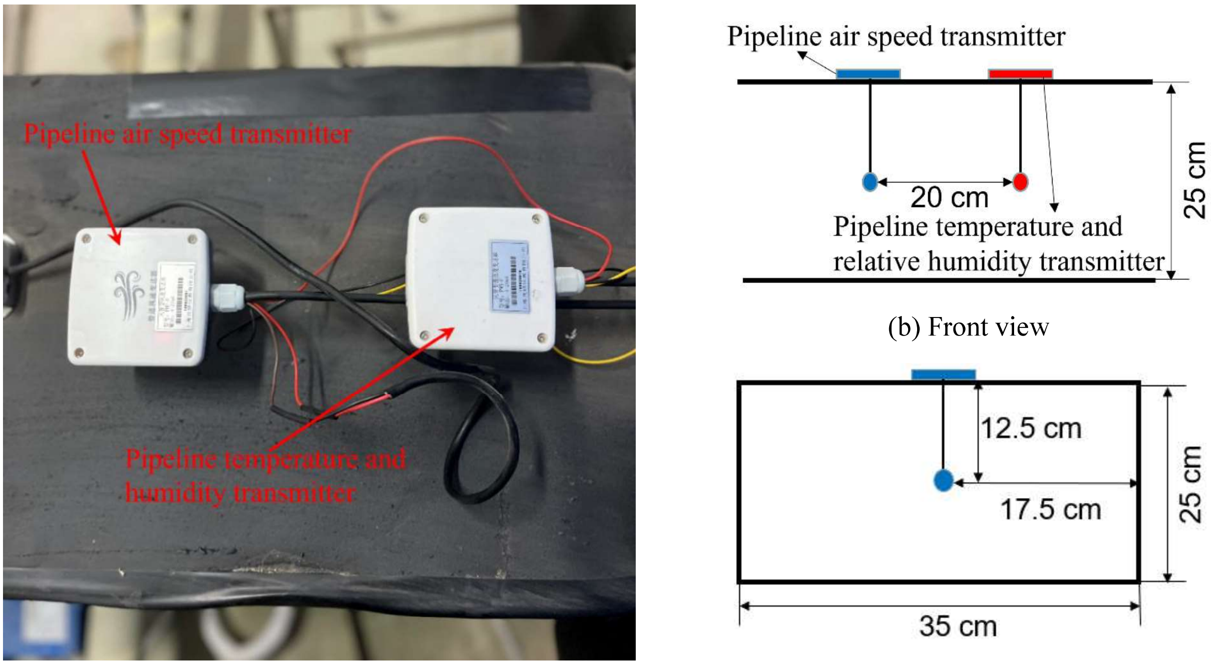

(a) Overhead shot of the site (c) Left view

Fig. 7. Measurement points of outlet air speed, OAT and OAH.

Fig. 7 illustrates the layout of the measurement points for air velocity, outlet air temperature (OAT), and outlet air relative humidity (OAH) after CDEC treatment. Fig. 7(a) shows an overhead shot of the site. In Fig. 7(b), the processed air first passes through the airspeed transmitter, followed by the temperature and humidity transmitter, with a distance of 20 cm between them. In Fig. 7(c), the air duct measures 35cm x 25cm. Both measurement points are positioned 12.5 cm from the top of the air duct and 17.5 cm from the side.

2.4. Experimental uncertainty

In the present work, the uncertainty of the experimental data was calculated using the methods proposed by Kline and Moffat [43,44], the relationship between variable K and the independent variable $x_1, x_2 \dots x_n$ is represented as follows:

$$K = f(x_1, x_2 \dots x_n) \tag{4}$$

The uncertainty calculation formula for variable K is as follows [45]:

$$\sigma_K = \sqrt{(\frac{\partial K}{\partial x_1}\sigma_{x_1})^2 + (\frac{\partial K}{\partial x_2}\sigma_{x_2})^2 + \cdots (\frac{\partial K}{\partial n}\sigma_{x_n})^2} = \sqrt{\sum_1^n (\frac{\partial K}{\partial x_i}\sigma_{x_i})^2} \tag{5}$$

where σ_{x_1},$\sigma_{x_2} \dots \sigma_{x_n}$ are the uncertainties of $x_1, x_2 \dots x_n$, respectively.

The uncertainty of measurement and calculation parameters in the experiment is listed in Table 2.

Table 2. Parameter uncertainty

Item	Units	Uncertainty
Measured parameters		
IAT	℃	± 0.01 ℃
OAT	℃	± 0.01 ℃
IAH	%	± 2% RH

OAH	%	± 2% RH
Air speed	m/s	± 0.02 %
Calculated parameters		
IAT and OAT difference	℃	± 0.014 ℃
Cooling capacity of CDEC	kW	± 0.089 kW
Energy consumption of air conditioning units	kW	± 0.057 kW
Energy saving rate	%	± 0.52 %

2.5. Experimental conditions

China's "East Calculation and West Calculation" national project has planned ten DC clusters. Table 3 provides basic information on these clusters. Meteorological analysis of the ten DC clusters reveals that the highest temperature in Chongqing is 37.7 ℃. As a result, the highest simulated temperature in the experiment is set at 37 ℃. According to the 2021 version of the DC Guidelines published by ASHRAE [46], the recommended supply air temperature in DCs should range between 18 ℃ and 27 ℃. Therefore, the simulated air temperature range for the experiment is 27 ℃ to 37 ℃. Meteorological data also indicate that air relative humidity tends to be low at higher air temperature. Li et al. [47] found that natural air with a relative humidity below 40% can meet DC air supply conditions after being cooled by CDEC. The air parameters used in this study are detailed in Table 4.

Table 3. Basic information of the ten DC clusters cities in China

Number	City	Latitude	Longitude	Climate zone	Annual average temperature/℃	Annual average relative humidity/%
1	Chengdu	30.5N	104.0E	Hot summer & warm winter	16.3	83
2	Shaoguan	23.1N	113.3E	Hot summer & warm winter	22.2	81
3	Wuhu	31.2N	118.2E	Hot summer & warm winter	15.5	61
4	Chongqing	29.2N	106.7E	Hot summer & warm winter	17	75
5	Guiyang	26.5N	106.2E	Mild	15.3	77
6	Qingyang	35.7N	107.5E	Cold	9.6	51
7	Hohhot	40.5N	111.7E	Severe cold	5.7	45
8	Shanghai	31.4N	121.4E	Hot summer & cold winter	17.7	71
9	Zhangjiakou	41.5N	115.0E	Hot summer & cold winter	9	60
10	Zhongwei	37.5N	105.0E	Hot summer & cold winter	8.4	57

Table 4. Parameter table of simulated high-temperature air conditions

Number	A	B	C	D	E	F
Temperature (℃)	27	29	31	33	35	37
Relative humidity (%)	38	36	34	32	30	28

2.5.1 The effect of spray angle on CDEC

During the experiment, the airspeed in the spray chamber was adjusted to 2.44 m/s using a frequency converter, while the spray flow rate was controlled at 0.8 L/min by adjusting the rotameter. Inlet air parameters C and D from Table 4 were selected, and the modular air-cooled heat pump unit was activated via the control platform. The water supply temperature to the heat exchanger was adjusted to heat the outdoor fresh air to the required temperature, with fluctuations not exceeding 0.2 ℃. Municipal water, with a stable pressure and temperature of 25 ℃± 0.5 ℃, was used as the spray water throughout the experiment. The spray angle was varied to 5°, 25°, 45°, 65°, and 85° for a total of 10 experiments. Data from the experiment were recorded at 10-second intervals using a data acquisition instrument. After the air temperature and relative humidity stabilized following CDEC cooling, the system was turned off, completing one set of experiments. A 10-minute interval was observed between experiments to prevent the residual field in the test bench from affecting subsequent trials.

2.5.2 The impact of air speed on CDEC

This section investigates the effect of airspeed on CDEC with a controlled spray flow rate of 0.8 L/min. The spraying angle is set to the optimal angle determined in the experiment under the conditions outlined in Section 2.4.1. Based on Table 4, set the IAT and IAH were set, and the the airspeed was adjusted to 1.53 m/s, 1.99 m/s, 2.44 m/s, 2.89 m/s, and 3.29 m/s using the frequency converter. A total of 30 test sets were conducted.

2.5.3 The impact of spray flow rate on CDEC

The spray flow rate plays a critical role in the performance of CDEC. Based on Table 4, the IAT and IAH were set, and the spray angle and airspeed were adjusted to their optimal values, as determined in Sections 2.4.1 and 2.4.2. The spray flow rate was then varied to 0.6 L/min, 0.7 L/min, 0.8 L/min, 0.9 L/min, and 1.0 L/min, resulting in a total of 30 experiments.

3. Experimental results

3.1. Impact of spray angle on CDEC

Based on the settings in Section 2.4.1, air conditions C and D from Table 4 were selected for testing. The spray angle was adjusted to 5°, 25°, 45°, 65°, and 85° to investigate the influence of spray angle on CDEC. Fig. 8 illustrates the changes in OAT and OAH with increasing spray angle.

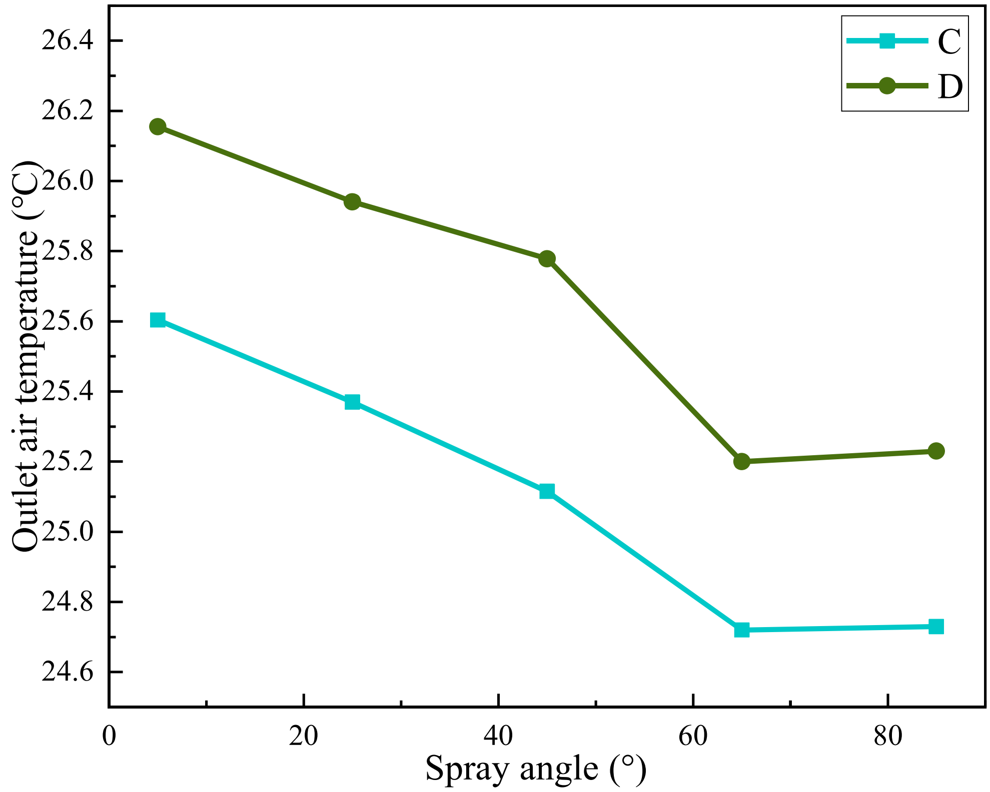

(a) Graph of the change of OAT with spray angle

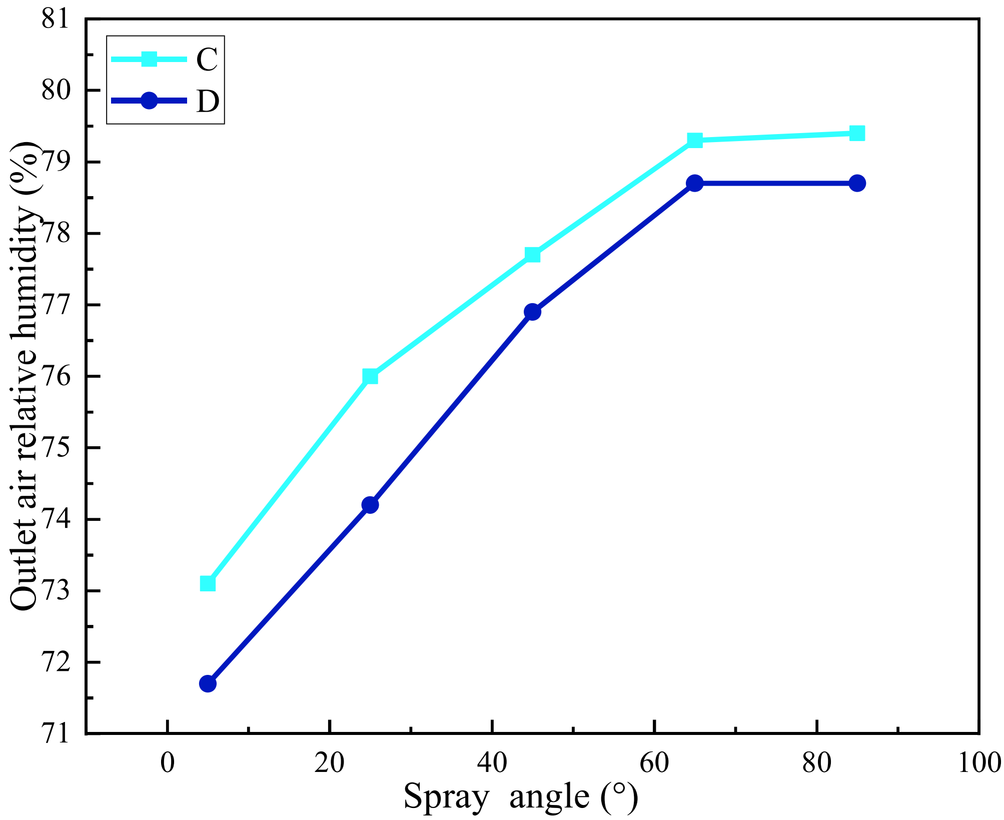

(b) Graph of the change of OAH with spray angle

Fig. 8. Impact of spray angle on CDEC.

(a) Change the spray angle to 45° (b) Change the spray angle to 85°

Fig. 9. Spray angle diagram.

Fig. 8 (a) shows that when the IAT is set at 31 ℃ and 33 ℃, increasing the spray angle enhances the contact time and contact area between air and water mist, thereby increasing heat exchange and causing the OAT to vary with the spray angle. The trend in OAT remains consistent with changes in spray angle. At a spray angle of 65 °, the outlet air temperature reaches its lowest point, measuring 24.72 ℃ and 25.20 ℃, respectively, resulting in temperature drops of 6.28 ℃ and 7.8 ℃. The experimental results from Shao et al. [38] indicated that air temperature decreases by approximately 7.2 ℃ following spray cooling, which supports the reliability of these findings. As shown in Fig. 8 (b), the OAH gradually increases as the spray angle increases from 5° to 65°. However, when the spray angle is increased to 65° and 85°, the relative humidity remains nearly constant, suggesting that 65° is the optimal spray angle. The contact area and time between air and cold mist are critical factors influencing the cooling performance of CDEC [48]. Fig. 9 (a) illustrates that cold mist is sprayed from the nozzle at a wide angle. As the spray angle increases, the contact area enlarges, allowing cold mist to cover a broader space within the spray chamber. Additionally, due to gravity, the cold mist sprayed by the nozzle moves downward, which increases the contact time between the air and cold mist as the spray angle increases. Consequently, as the spray angle increases, the air temperature continues to decrease while the relative humidity increases. It can be seen from Fig. 9 (b) that when the spray angle is increased to 85°, some of the water mist condenses on the top surface, resulting in reduced cold mist availability. This decrease diminishes heat and moisture exchange, leading to a slight increase in OAT.

3.2. Impact of air speed on CDEC

Based on the settings in Section 2.4.2, the spray angle was set to 65°, and the spray flow rate was adjusted to 0.8 L/min. The air parameters for the experiment were set to A-F as listed in Table 4, and the air speeds were adjusted to 1.53 m/s, 1.99 m/s, 2.44 m/s, 2.89 m/s, and 3.29 m/s. Fig. 10 illustrates the changes in OAT and OAH after processing various high-temperature air at these different air speeds.

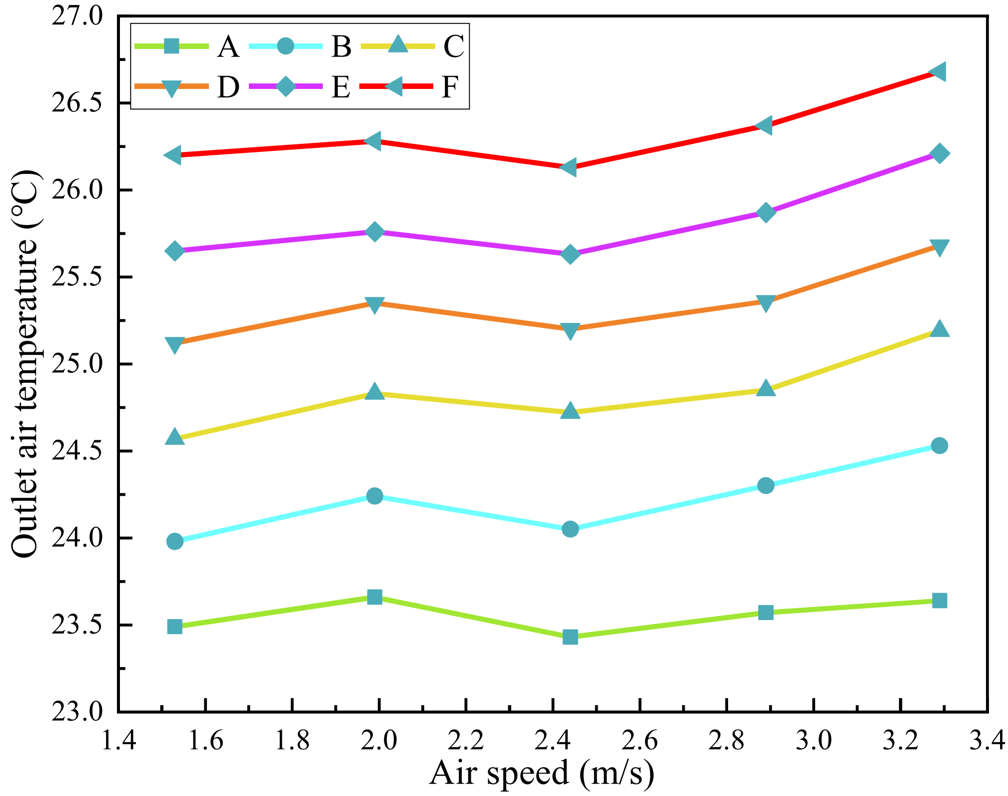

(a) Variation of OAT with air speed

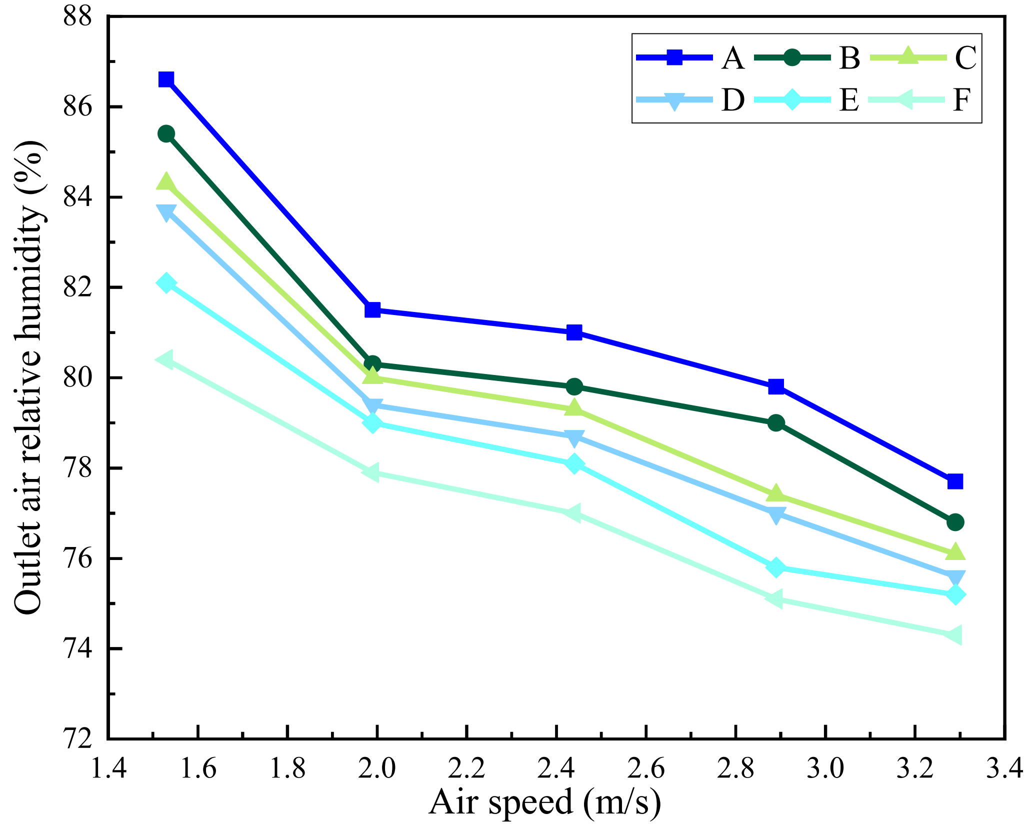

(b) Variation of OAH with air speed

Fig. 10. Impact of air speed on CDEC.

As shown in Fig. 10(a), the trend in OAT is almost remains relatively consistent across different IAT as air speed increases. The OAT initially increases, then decreases, and subsequently increases as air speed increases from 1.53 m/s to 3.29 m/s. At an air speed of 1.53 m/s, the airflow into the spray chamber is low, allowing for sufficient heat and moisture exchange between the air and cold mist. This results in a significant temperature drop, while the OAH remains relatively high. From Fig. 10(b), as the air speed increases to 1.99 m/s, the OAT increases and the OAH decreases. This change occurs since the greater airflow into the spray chamber shortens the contact time between the air and cold mist, weakening heat and moisture exchange. At an air speed of 2.44m/s, the interaction between the air and cold mist intensifies, enhancing convective heat transfer and optimising heat and humidity exchange. At this point, the OAT reaching its lowest value, while the OAH satisfies the air supply conditions for the DC. Thus, an air speed of 2.44 m/s is identified as optimal for treating air with CDEC. As the air speed increases further to 2.89 m/s and 3.29 m/s, the OAT continues to increase and the OAH decreases. This is due to the fact that a higher air speed results in a larger volume of air entering the spray chamber, which limits the cold mist's ability to effectively exchange heat and moisture with the air. Additionally, the contact time between the air and cold mist decreases as air velocity increases. Therefore, in practical engineering applications, the optimal operating air speed for CDEC units of varying sizes can be determined through trial operations, allowing for adjustments to the number of cooling devices based on the required air supply for the DC.

To demonstrate that the increase in OAT at high air speeds is due to insufficient cold mist for effective heat and moisture exchange, this study conducted supplementary experiments with a spray flow rate increased to 0.9 L/min at air speeds of 2.89 m/s and 3.29 m/s. The results of these supplementary experiments were then compared with thoses presented in Fig. 10.

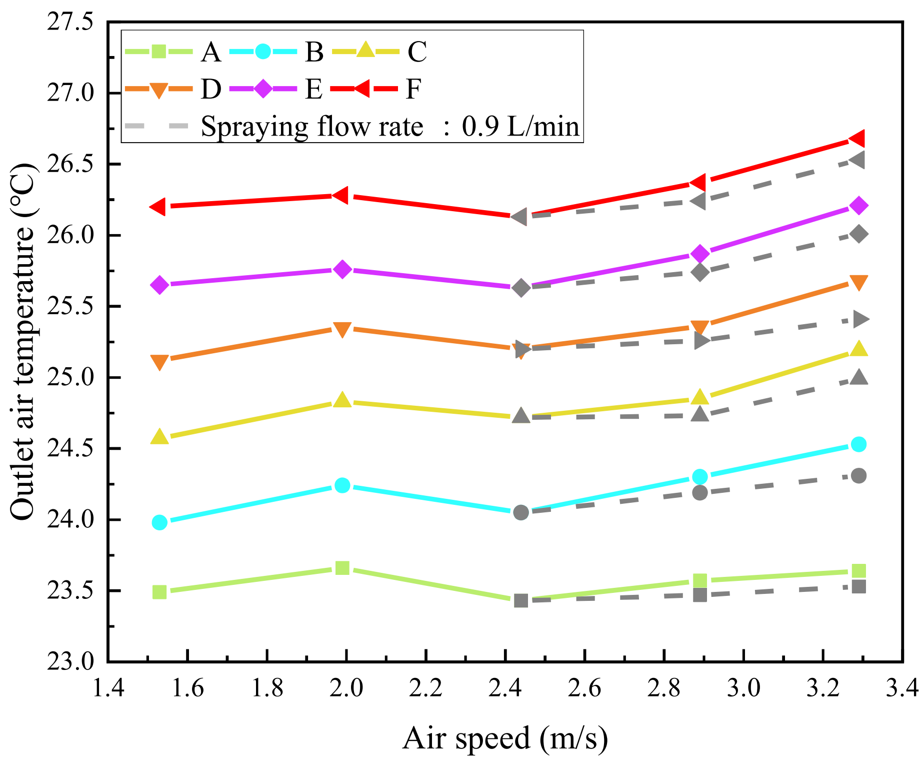

(a) Change chart of OAT for increasing spray flow rate

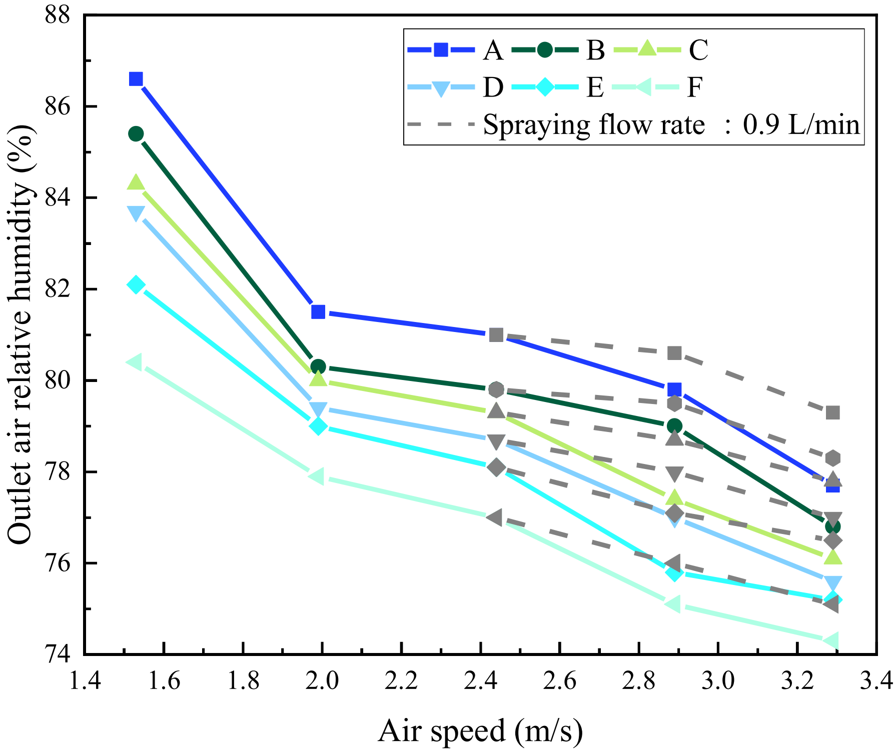

(b) Change chart of OAH for increasing spray flow rate

Fig. 11. Change chart of OAT and OAH for increasing spray flow rate

The experimental results in Fig. 11 show that with a spray flow rate of 0.9 L/min, compared to Fig. 10, the OAT decreases and the OAH increases at air speeds of 2.89 m/s and 3.29 m/s when air conditions from Table 4 are treated with CDEC. This occurs because, at higher air speeds, increasing the spray flow rate could enhance heat and moisture exchange. These results confirm that the explanation for the increase in OAT in Fig. 10(a) at air speeds of 2.89 m/s and 3.29 m/s is correct.

3.3. Impact of spray flow rate on CDEC

Following the setup in Section 2.3.3, the spray angle was set to 65° and the airspeed to 2.44m/s. The air parameters for the experiment were set to A-F as listed in Table 4, and the spray flow rate was adjusted to 0.6 L/min, 0.7 L/min, 0.8 L/min, 0.9 L/min, and 1.0 L/min. Fig. 12 shows the changes in OAT and OAH after CDEC treatment of different high-temperature air under varying spray flow rates.

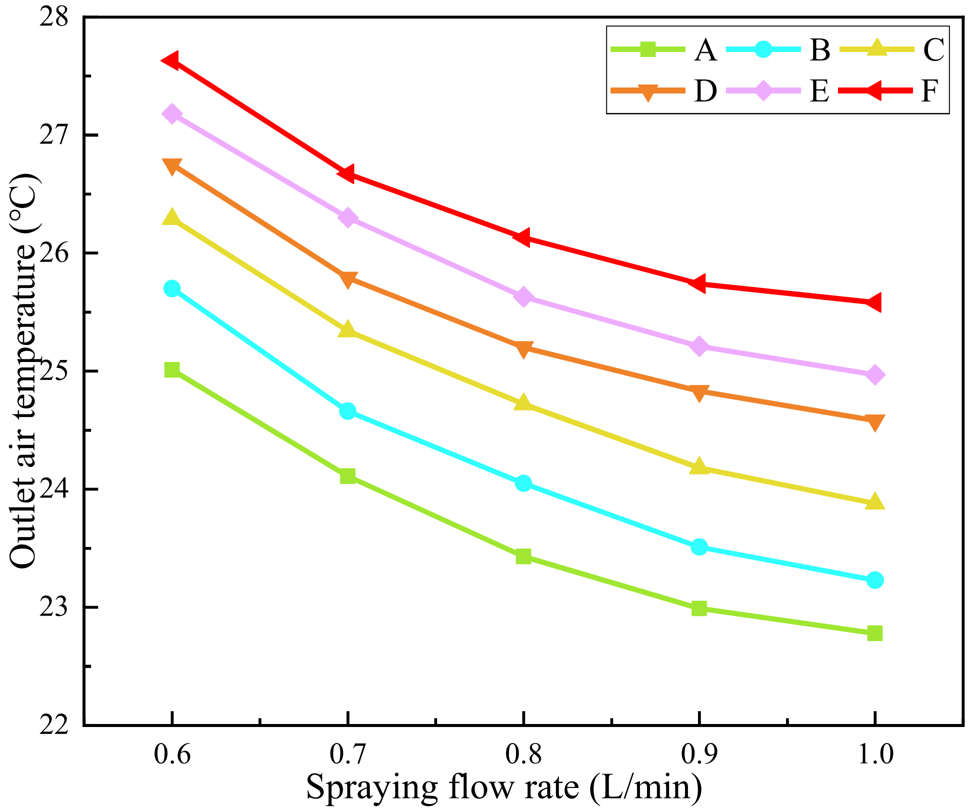

(a) Variation of OAT with spray flow rate

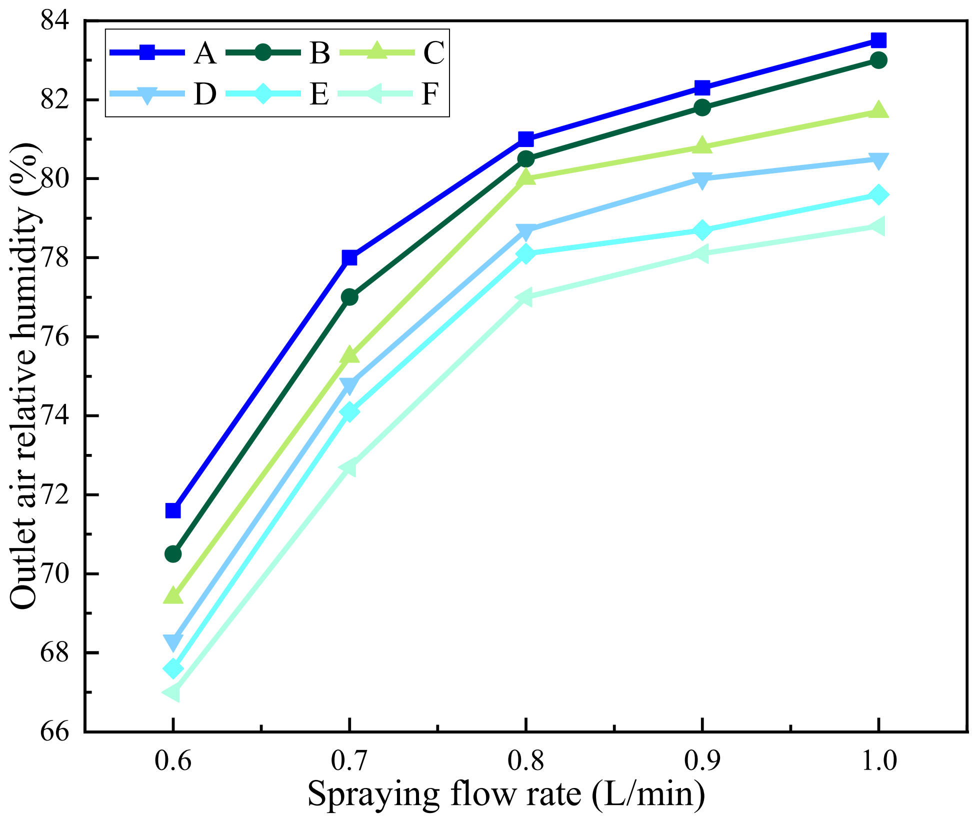

(b) Variation of OAH with spray flow rate

Fig. 12. Impact of spray flow rate on CDEC.

As shown in Fig. 12(a) and (b), the trends of OAT and OAH for air cooled by CDEC at different temperatures follow a similar pattern across varying spray velocities. As the spray flow rate increases, OAT decreases and OAH increases. This is because with more cold mist entering the spray chamber, and the airspeed remaining constant, the air undergoes enhanced cooling by the additional cold mist. Consequently, OAT continues to drop while OAH increases. Although a higher spray flow rate results in lower air temperature, it also leads to higher relative humidity, especially when the IAH is high. This is because ideal direct evaporative cooling follows the adiabatic saturation process [49], where the limiting temperature is the wet-bulb temperature of the air [50]. In such conditions, the relative humidity of the outlet air can reach up to 100%. As shown in Fig. 12 (b), when the spray flow is high, the OAH may exceed the allowable humidity range for DC after the low-temperature, high-humidity air is treated by CDEC. Therefore, in practical applications, selecting a lower spray flow rate is advisable to maintain the desired humidity levels.

4. Discussion

4.1. Application analysis

Based on the experiment results, high-temperature air ranging from 27 ℃ to 37 ℃ can be cooled to 23.57 ℃ to 25.58 ℃, with a relative humidity between 67.0% and 78.8% using CDEC. According to ASHRAE guidelines, the recommended supply air temperature for DCs is between 18 ℃ and 27 ℃, with an allowable relative humidity of 8% to 80% for A1 DCs. In this study, the high-temperature air was successfully treated with CDEC to meet the air supply requirements for DCs in terms of both temperature and humidity. These findings demonstrate the feasibility of using CDEC to provide natural cooling for DCs in hot climates. Unlike previous studies that primarily employed evaporative cooling to supplement traditional vapor-compression refrigeration systems [38,51], this study directly utilises CDEC to deliver natural cooling for DCs. This approach not only reduces the cost associated with traditional refrigeration equipment but also enhances the use of natural cooling sources in DCs. Additionally, the cold air produced by CDEC could be applied to other large-scale environments requiring cooling, such as airports, train stations, and subway stations.

Air speed plays a crucial role in the performance of CDED-treated air. In this study, the experiment described in Section 3.2 was designed to determine the optimal intake air speed at different temperatures under CDEC conditions. The experimental results from Section 3.2 show that the trends of OAT and OAH remain consistent across various high-temperature air treatments, with the lowest OAT occurring at an air speed of 2.44 m/s. Therefore, when the spray flow rate is set to 0.8 L/min, the optimal air speed is 2.44m/s. Notably, the optimal air speed is not influenced by the temperature of the treated air but represents a system-specific optimal air speed for the CDEC process.

The spray flow rate also significantly impacts the performance of CDEC. Based on the experimental results from Section 3.3, the trend of OAT remains consistent across various high-temperature air treatments as the spray flow rate increases. As the spray flow rate increases, the treated air temperature decreases, while the relative humidity increases. Although lower air temperatures are desirable for cooling DCs, an excessive spray flow rate can cause relative humidity levels to exceed the maximum allowable limits for DC supply air. Additionally, higher spray flow rates increase water consumption, leading to resource waste. Therefore, in practical engineering applications, it is essential to adjust the spray flow rate according to the natural air conditions to achieve the desired low-temperature air without exceeding humidity constraints.

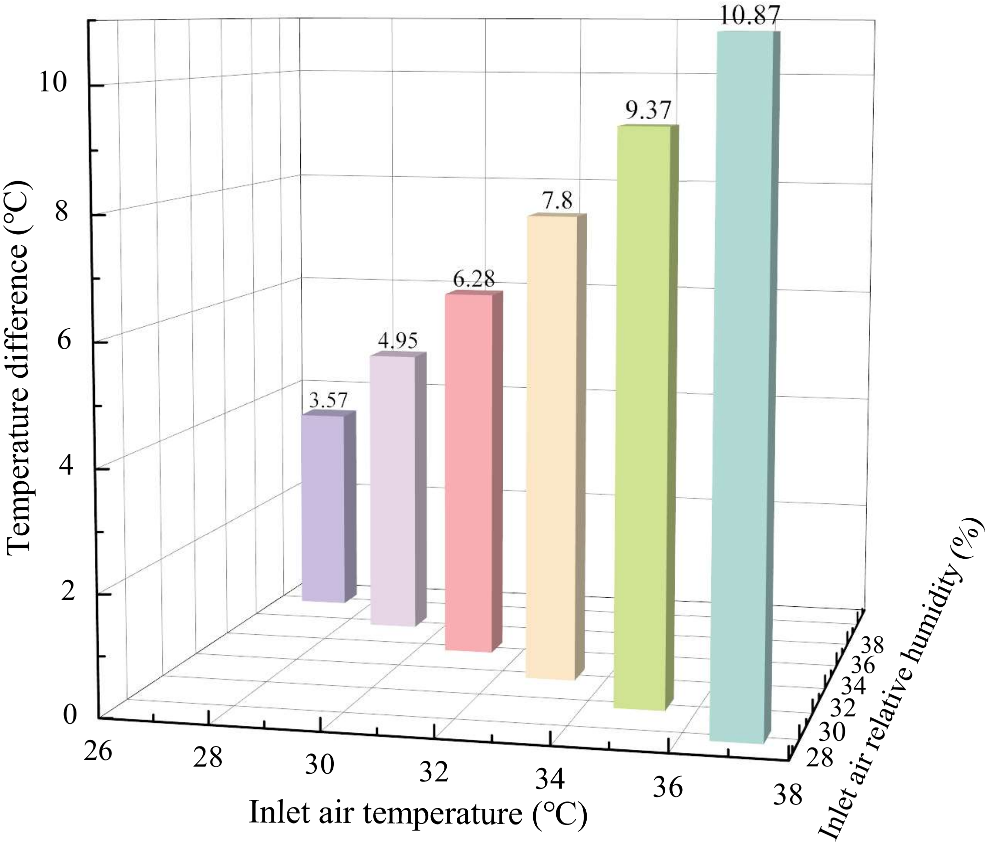

Fig. 13. Variation of the temperature difference between the IAT and the OAT.

$$\Delta t = IAT - OAT \tag{6}$$

where Δt is the temperature difference between IAT and OAT; IAT is the inlet air temperature, °C; OAT is the outlet air temperature, °C.

To assess the cooling effect of air at different temperatures after CDEC treatment, experiments in Sections 3.2 and 3.3 were conducted using a spray flow rate of 0.8 L/min and an air speed of 2.44 m/s. The temperature difference between the inlet air and outlet air was calculated using Eq. (6). Based on these calculations, a temperature difference variation chart between IAH and OAT was created, as shown in Fig. 13. According to Fig. 13, the temperature difference between IAT and OAT ranges from 3.57 °C to 10.87 °C, indicating a strong cooling capacity. The temperature difference increases with the increase of OAT and decreases with the decrease of IAH. These results demonstrate that CDEC is highly effective at cooling high-temperature, low-humidity air, highlighting its significant potential for application in regions with such conditions. This suggests that the use of natural cooling sources in DCs could increase further in these areas.

4.2. Energy efficiency

By comparing the energy consumption of CDEC with that of the modular air-cooled heat pump unit in Table 1, the energy-saving rate of CDEC for producing the same cooling capacity can be determined. During the CDEC process, only the fan consumes energy. Based on the frequency converter data, at an air speed of 2.44 m/s, the fan's energy consumption is 1.1 kW. In contrast, the modular air-cooled heat pump unit is equipped with a pump that consumes 1.1 kW of energy. The modular air-cooled heat pump unit also requires electricity for refrigeration, with a coefficient of performance (COP) of 3.27, as shown in Table 1. The cooling capacity generated by CDEC is calculated using Eq. (7), while the energy consumption of the modular air-cooled heat pump unit for the same cooling capacity is determined using Eq. (8). Finally, the energy-saving rate of CDEC compared to the modular air-cooled heat pump unit can be calculated using Eq. (9).

$$Q = \rho \cdot v \cdot s \cdot c_{pm} \cdot \Delta t = Q_x \tag{7}$$

$$W = \frac{Q}{\eta} + Q_p \tag{8}$$

$$\xi = \frac{W - Q_f}{W} \times 100\% \tag{9}$$

where Q is the cooling capacity prepared by CDEC, kW; ρ is the air density, which takes 1.20 kg/m³; v is the air speed, m/s; s represents the cross-sectional area of air duct, is 0.0878 m^2; c_{pm} is the specific heat capacity of air, which takes 1.003 kJ/(kg·°C); Q_p is the water pump energy consumption of the modular air-cooled heat pump unit, kW; W is the energy consumption of the modular air-cooled heat pump unit, kW; η is the refrigeration coefficient; ξ is the energy saving rate of CDEC; Q_f is the energy consumption of the fan of the air supply system, kW.

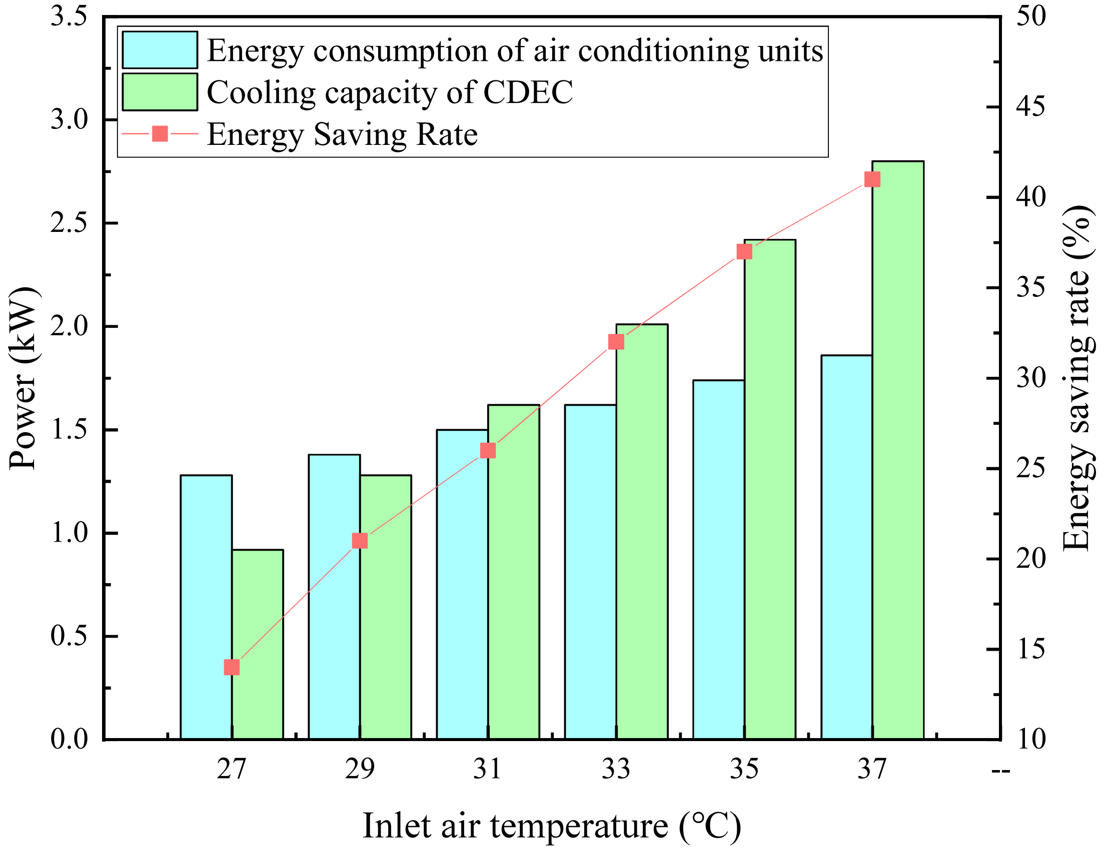

Fig. 14. Comparison of energy consumption of CDEC and modular air-cooled heat pump units.

As shown in Fig. 14, using CDEC for DC cooling can achieve energy savings of 14% to 41% compared to a modular air-cooled heat pump unit for the same cooling capacity. The higher the natural air temperature and the lower the relative humidity, the energy-saving effect becomes more pronounced. When the temperature is below 27 °C, DCs can rely solely on natural air for cooling. For temperature above 27 °C, natural air cooling can still be utilized with the assistance of CDEC. Therefore, implementing a hybrid cooling system that combines direct air cooling with CDEC will significantly reduce the energy consumption of DCs, contributing to substantial energy savings and emission reductions.

4.3. Free cooling time throughout the year

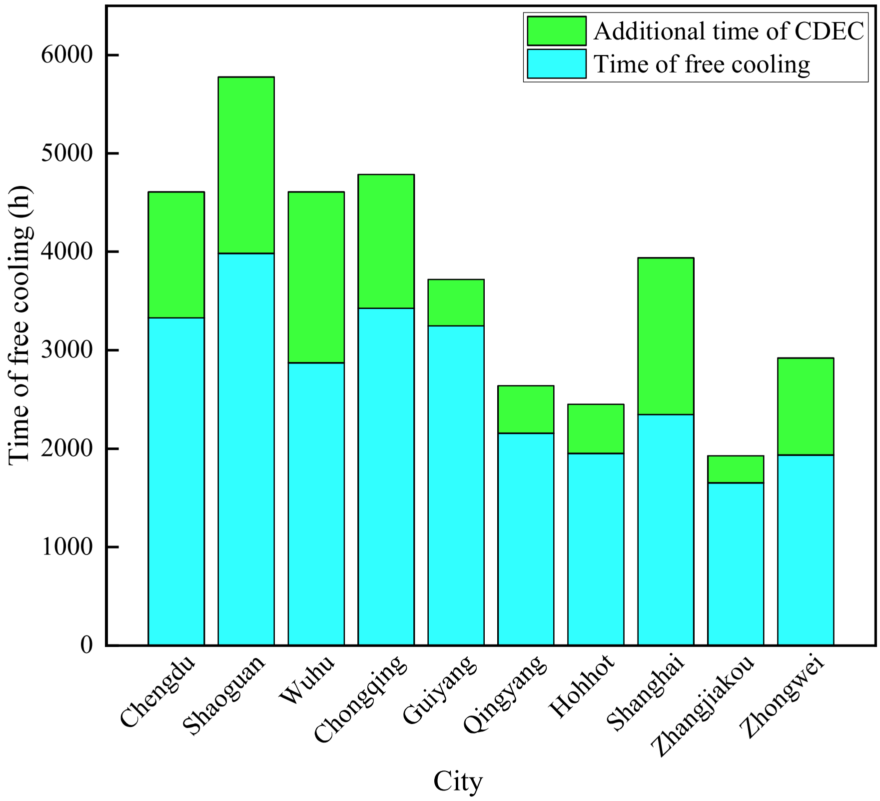

Fig. 15. Statistics of high temperature meteorological data and its proportion in the whole year.

Annual free cooling time refers to the duration during which DCs can utilise natural cooling sources for cooling during operation. During the free cooling, the DC cooling system does not use electric cooling, which can significantly reduce the energy consumption. It is concluded that when the natural air temperature exceeds 27 °C, CDEC can be employed to meet the cooling requirements of DCs. To quantify the improvement in annual free cooling time with CDEC technology in DCs, a statistical analysis of meteorological data from the top ten DC clusters in China was conducted, as shown in Fig. 15. The results indicate that implementing CDEC in DCs can extend the annual free cooling time by 3.16% to 20.45%, depending on the location.

5. Conclusions

Cold-mist Direct Evaporative Cooling (CDEC) is an effective and low-cost cooling technology. This study examined the treatment of various high-temperature air using CDEC and explored the impacts of several key control parameters such as spray angle, air speed, and spray flow rate, on the CDEC process across different air temperature. The key research findings are as follows:

(1) In the CDEC system, the obtained optimal spray angle is 65°;

(2) When cooling fresh air at various temperatures using CDEC, the optimal air speed is 2.44 m/s. As the spray flow rate increases, a lower outlet air temperature after CDEC treatment corresponds to a higher relative humidity;

(3) By adjusting the air speed and spray flow rate, high-temperature air in the range of 27 ℃ to 37 ℃ can be cooled to between 23.57 ℃ and 25.58 ℃ after CDEC treatment, with relative humidity levels between 67.0% and 78.8%, thereby meeting the air supply requirements for DCs. Generally, higher air temperatures correspond to lower humidity levels, which enhances the cooling effect;

(4) Compared to modular air-cooled heat pump units, the implementation of CDEC technology in DCs can achieve energy savings of 14% to 41%;

(5) The implementation of CDEC can extend the annual free cooling time of DCs in China by 3.16% to 20.45%.

This study highlights the potential of CDEC as a supplementary cooling source for the direct air cooling systems of DCs in high-temperature climates. By addressing the challenge of high energy consumption in DC cooling systems, CDEC significantly reduces the power usage effectiveness (PUE) of these facilities. Implementing this research method can effectively lower energy consumption, reducing operating costs, and foster the growth of the industry. Additionally, the findings of this study could be applicable to other large spaces that require cooling, such as airports, train stations, and subway stations. The analysis and discussion presented indicate that the results of this research are of considerable importance. However, this study primarily focuses on whether the temperature and humidity conditions of high-temperature air treated by CDEC can meet the air supply requirements for DCs. Future research should explore the practical application of CDEC in DCs, which will be influenced by various factors. Changes in the actual implementation of CDEC in DCs can be investigated through experiments or numerical simulations, enhancing the applicability of these findings to real-world engineering challenges. Furthermore, subsequent research should consider how CDEC performance varies under dynamic temperature changes.

Declaration of Competing Interests

The authors declare that they have no known competing financial interests or personal relationships that could have appeared to influence the work reported in this paper.

Acknowledgments

The author would like to thank the financial support of the National Natural Science Foundation of China (NO. 52168013), and the Guizhou Provincial Science and Technology Projects (No. ZK [2022]151 and [2019]1102).

References

[1] K. Ebrahimi, G.F. Jones, A.S. Fleischer, A review of DC cooling technology, operating conditions and the corresponding low-grade waste heat recovery opportunities, Renewable and Sustainable Energy Reviews. 31 (2014) 622-638, https://doi.org/10.1016/j.rser.2013.12.007.

[2] E. Masanet, A. Shehabi, N. Lei, S. Smith, J. Koomey, Recalibrating global DC energy-use estimates, Science. 367 (6481) (2020) 984-986, 10.1126/science.aba3758.

[3] H. Zhu, D. Zhang, H.H. Goh, S. Wang, T. Ahmad, D. Mao, T. Liu, H. Zhao, T. Wu, Future DC energy-conservation and emission-reduction technologies in the context of smart and low-carbon city construction, Sust. Cities Soc. 89

(2023) 104322, https://doi.org/10.1016/j.scs.2022.104322.
[4] IEA, Electricity 2024, in: INTERNATIONAL ENERGY AGENCY, 2024, p. 31.
[5] C. Jin, X. Bai, C. Yang, W. Mao, X. Xu, A review of power consumption models of servers in DCs, Appl. Energy. 265 (2020) 114806, https://doi.org/10.1016/j.apenergy.2020.114806.
[6] K. Sun, N. Luo, X. Luo, T. Hong, Prototype energy models for DCs, Energy Build. 231 (2021) 110603, https://doi.org/10.1016/j.enbuild.2020.110603.
[7] M.U.A. K., S. J., H.J.B. M., K.R. S., Electrical Energy Consumption Model of Internal Components in DCs, in: 2019 IEEE PES Innovative Smart Grid Technologies Europe (ISGT-Europe), 2019, pp. 1-5.
[8] L. Liu, Q. Zhang, Z.J. Zhai, C. Yue, X. Ma, State-of-the-art on thermal energy storage technologies in DC, Energy Build. 226 (2020) 110345, https://doi.org/10.1016/j.enbuild.2020.110345.
[9] T.L. Vasques, P. Moura, A. de Almeida, A review on energy efficiency and demand response with focus on small and medium DCs, Energy Effic. 12 (5) (2019) 1399-1428, 10.1007/s12053-018-9753-2.
[10] Y. Zhang, K. Shan, X. Li, H. Li, S. Wang, Research and Technologies for next-generation high-temperature DCs – State-of-the-arts and future perspectives, Renewable and Sustainable Energy Reviews. 171 (2023) 112991, https://doi.org/10.1016/j.rser.2022.112991.
[11] D. Al Kez, A.M. Foley, D. Laverty, D.F. Del Rio, B. Sovacool, Exploring the sustainability challenges facing digitalization and internet DCs, J. Clean. Prod. 371 (2022) 133633, https://doi.org/10.1016/j.jclepro.2022.133633.
[12] Y. Liu, X. Wei, J. Xiao, Z. Liu, Y. Xu, Y. Tian, Energy consumption and emission mitigation prediction based on DC traffic and PUE for global DCs, Global Energy Interconnection. 3 (3) (2020) 272-282, https://doi.org/10.1016/j.gloei.2020.07.008.
[13] K. Cho, H. Chang, Y. Jung, Y. Yoon, Economic analysis of DC cooling strategies, Sust. Cities Soc. 31 (2017) 234-243, https://doi.org/10.1016/j.scs.2017.03.008.
[14] M. Koot, F. Wijnhoven, Usage impact on DC electricity needs: A system dynamic forecasting model, Appl. Energy. 291 (2021) 116798, https://doi.org/10.1016/j.apenergy.2021.116798.
[15] A.M. Abbas, A.S. Huzayyin, T.A. Mouneer, S.A. Nada, Thermal management and performance enhancement of DCs architectures using aligned/staggered in-row cooling arrangements, Case Stud. Therm. Eng. 24 (2021) 100884, https://doi.org/10.1016/j.csite.2021.100884.
[16] Y. Lee, C. Wen, Y. Shih, Z. Li, A. Yang, Numerical and experimental investigations on thermal management for DC with cold aisle containment configuration, Appl. Energy. 307 (2022) 118213, https://doi.org/10.1016/j.apenergy.2021.118213.
[17] X. Meng, J. Zhou, X. Zhang, Z. Luo, H. Gong, T. Gan, Optimization of the thermal environment of a small-scale DC in China, Energy. 196 (2020) 117080, https://doi.org/10.1016/j.energy.2020.117080.
[18] H. Moazamigoodarzi, R. Gupta, S. Pal, P.J. Tsai, S. Ghosh, I.K. Puri, Modeling temperature distribution and power consumption in IT server enclosures with row-based cooling architectures, Appl. Energy. 261 (2020) 114355, https://doi.org/10.1016/j.apenergy.2019.114355.
[19] M.H.B. Mahbod, C.B. Chng, P.S. Lee, C.K. Chui, Energy saving evaluation of an energy efficient DC using a model-free reinforcement learning approach, Appl. Energy. 322 (2022) 119392, https://doi.org/10.1016/j.apenergy.2022.119392.
[20] I. Keskin, G. Soykan, Optimal cost management of the CCHP based DC with district heating and district cooling integration in the presence of different energy tariffs, Energy Conv. Manag. 254 (2022) 115211, https://doi.org/10.1016/j.enconman.2022.115211.
[21] Q. Tian, Q. Guo, S. Nojavan, X. Sun, Robust optimal energy management of DC equipped with multi-energy conversion technologies, J. Clean. Prod. 329 (2021) 129616, https://doi.org/10.1016/j.jclepro.2021.129616.
[22] Y. Zhang, C. Li, M. Pan, Design and performance research of integrated indirect liquid cooling system for rack server,

Int. J. Therm. Sci. 184 (2023) 107951, 10.1016/j.ijthermalsci.2022.107951.

[23] P. Huang, B. Copertaro, X. Zhang, J. Shen, I. Löfgren, M. Rönnelid, J. Fahlen, D. Andersson, M. Svanfeldt, A review of DCs as prosumers in district energy systems: Renewable energy integration and waste heat reuse for district heating, Appl. Energy. 258 (2020) 114109, https://doi.org/10.1016/j.apenergy.2019.114109.

[24] S. Kwon, Ensuring renewable energy utilization with quality of service guarantee for energy-efficient DC operations, Appl. Energy. 276 (2020) 115424, https://doi.org/10.1016/j.apenergy.2020.115424.

[25] M.H. Jahangir, R. Mokhtari, S.A. Mousavi, Performance evaluation and financial analysis of applying hybrid renewable systems in cooling unit of DCs – A case study, Sustain. Energy Technol. Assess. 46 (2021) 101220, https://doi.org/10.1016/j.seta.2021.101220.

[26] J. Ding, H. Zhang, D. Leng, H. Xu, C. Tian, Z. Zhai, Experimental investigation and application analysis on an integrated system of free cooling and heat recovery for DCs, Int. J. Refrig. 136 (2022) 142-151, 10.1016/j.ijrefrig.2022.01.003.

[27] P. Guo, S. Wang, Y. Lei, J. Li, Numerical simulation of solar chimney-based direct airside free cooling system for green DCs, J. Build. Eng. 32 (2020) 101793, https://doi.org/10.1016/j.jobe.2020.101793.

[28] F. Zhou, C. Shen, G. Ma, X. Yan, Power usage effectiveness analysis of a liquid-pump-driven hybrid cooling system for DCs in subclimate zones, Sustain. Energy Technol. Assess. 52 (2022) 102277, https://doi.org/10.1016/j.seta.2022.102277.

[29] M. Rampazzo, M. Lionello, A. Beghi, E. Sisti, L. Cecchinato, A static moving boundary modelling approach for simulation of indirect evaporative free cooling systems, Appl. Energy. 250 (2019) 1719-1728, https://doi.org/10.1016/j.apenergy.2019.04.087.

[30] U. Sajjad, N. Abbas, K. Hamid, S. Abbas, I. Hussain, S.M. Ammar, M. Sultan, H.M. Ali, M. Hussain, Tauseef-ur-Rehman, C.C. Wang, A review of recent advances in indirect evaporative cooling technology, Int. Commun. Heat Mass Transf. 122 (2021) 105140, https://doi.org/10.1016/j.icheatmasstransfer.2021.105140.

[31] X. Cui, W. Yan, X. Chen, Y. Wan, K.J. Chua, Parametric study of a membrane-based semi-direct evaporative cooling system, Energy Build. 228 (2020) 110439, https://doi.org/10.1016/j.enbuild.2020.110439.

[32] J. Tissot, P. Boulet, A. Labergue, G. Castanet, F. Trinquet, L. Fournaison, Experimental study on air cooling by spray in the upstream flow of a heat exchanger, Int. J. Therm. Sci. 60 (2012) 23-31, 10.1016/j.ijthermalsci.2012.06.005.

[33] Y.T. Liu, X. Yang, J.M. Li, X.D. Zhao, Energy savings of hybrid dew-point evaporative cooler and micro-channel separated heat pipe cooling systems for computer DCs, Energy. 163 (2018) 629-640, 10.1016/j.energy.2018.07.172.

[34] Z. Zhang, S. He, M. Yan, M. Gao, Y. Shi, Y. Lu, J. Liu, C. Guo, X. Huang, Numerical study on the performance of a two-nozzle spray cooling system under different conditions, Int. J. Therm. Sci. 152 (2020) 106291, 10.1016/j.ijthermalsci.2020.106291.

[35] A. Alkhedhair, I. Jahn, H. Gurgenci, Z. Guan, S. He, Parametric study on spray cooling system for optimising nozzle design with pre-cooling application in natural draft dry cooling towers, Int. J. Therm. Sci. 104 (2016) 448-460, 10.1016/j.ijthermalsci.2016.02.004.

[36] G. Cao, S. Zhang, Q. Zhang, G. Liu, X. Zhang, K. Yan, D. Chai, Experimental and numerical investigations of heat transfer characteristics of vertical falling film heat exchanger in DC cabinets, Int. Commun. Heat Mass Transf. 144 (2023) 106742, https://doi.org/10.1016/j.icheatmasstransfer.2023.106742.

[37] Z. Han, Q. Ji, H. Wei, D. Xue, X. Sun, X. Zhang, X. Li, Simulation study on performance of DC air-conditioning system with novel evaporative condenser, Energy. 210 (2020) 118521, https://doi.org/10.1016/j.energy.2020.118521.

[38] S. Shao, H. Liu, H. Zhang, C. Tian, Experimental investigation on a loop thermosyphon with evaporative condenser for free cooling of DCs, Energy. 185 (2019) 829-836, https://doi.org/10.1016/j.energy.2019.07.095.

[39] Y. Jing, X. Xie, Y. Jiang, Performance comparison and suitable climatic zones of three water-mediated evaporative cooling technologies, Energy Conv. Manag. 277 (2023) 116637, https://doi.org/10.1016/j.enconman.2022.116637.

[40] J.C. Kloppers, D.G. Kröger, The Lewis factor and its influence on the performance prediction of wet-cooling towers, Int. J. Therm. Sci. 44 (9) (2005) 879-884, https://doi.org/10.1016/j.ijthermalsci.2005.03.006.

[41] W. Zalewski, P.A. Gryglaszewski, Mathematical model of heat and mass transfer processes in evaporative fluid coolers, Chemical Engineering and Processing: Process Intensification. 36 (4) (1997) 271-280, https://doi.org/10.1016/S0255-2701(97)00006-8.

[42] I.L. Maclaine-cross, P.J. Banks, A General Theory of Wet Surface Heat Exchangers and its Application to Regenerative Evaporative Cooling, Journal of Heat Transfer. 103 (3) (1981) 579-585, 10.1115/1.3244505.

[43] S.J. Kline, F.A. Mcclintock, Describing Uncertainties in Single-Sample Experiments, Mechanical Engineering (New York, N.Y.: 1919). 75 (1) (1953).

[44] R.J. Moffat, Describing the uncertainties in experimental results, Exp. Therm. Fluid Sci. 1 (1) (1988) 3-17, https://doi.org/10.1016/0894-1777(88)90043-X.

[45] B. Du, Y. He, Y. Qiu, Q. Liang, Y. Zhou, Investigation on heat transfer characteristics of molten salt in a shell-and-tube heat exchanger, Int. Commun. Heat Mass Transf. 96 (2018) 61-68, https://doi.org/10.1016/j.icheatmasstransfer.2018.05.020.

[46] ASHRAE, Equipment Thermal Guidelines for Data Processing Enviroments,ed.Technical Committee(TC)9.9, in, 2021, p.

[47] C. Li, R. Mao, Y. Wang, J. Zhang, J. Lan, Z. Zhang, Experimental study on direct evaporative cooling for free cooling of DCs, Energy. 288 (2024) 129889, https://doi.org/10.1016/j.energy.2023.129889.

[48] Y.M. Xuan, F. Xiao, X.F. Niu, X. Huang, S.W. Wang, Research and application of evaporative cooling in China: A review (I) – Research, Renewable and Sustainable Energy Reviews. 16 (5) (2012) 3535-3546, https://doi.org/10.1016/j.rser.2012.01.052.

[49] S. Abdullah, M.N.B.M. Zubir, M.R.B. Muhamad, K.M.S. Newaz, H.F. Öztop, M.S. Alam, K. Shaikh, Technological development of evaporative cooling systems and its integration with air dehumidification processes: A review, Energy Build. 283 (2023) 112805, https://doi.org/10.1016/j.enbuild.2023.112805.

[50] H. Yan, Y. Chen, Y. Min, Y. Pan, An adaptive controller based dynamic simulation of household air-conditioner with indirect evaporative cooler as dedicated outdoor air system, Energy Build. 274 (2022) 112454, https://doi.org/10.1016/j.enbuild.2022.112454.

[51] S. Wang, R. Tu, X. Chen, X. Yang, K. Jia, Thermal performance analyses and optimization of DC centralized-cooling system, Appl. Therm. Eng. 222 (2023) 119817, https://doi.org/10.1016/j.applthermaleng.2022.119817.